

Enhancing the optical cross section of quantum antenna

Jingfeng Liu,^{1,2} Ming Zhou,² Lei Ying,² Xuewen Chen,³ and Zongfu Yu^{2,*}

¹College of Electronic Engineering, South China Agricultural University, Guangzhou 510642, China

²Department of Electrical and Computer Engineering, University of Wisconsin–Madison, Wisconsin 53706, USA

³School of Physics, Huazhong University of Science and Technology, Wuhan 430074, China

(Received 17 May 2016; published 6 January 2017)

The classical radio-frequency antenna theory indicates that large cross sections can be realized through directional radiation. In this paper, a similar principle is applied in quantum systems, in which quantum antennas, constructed by a cluster of quantum two-level systems, explore the collective excitation of two-level systems to realize large directivity. Both the optical cross section and the coherent time can be dramatically enhanced in free space, far exceeding the case of a single two-level system.

DOI: [10.1103/PhysRevA.95.013814](https://doi.org/10.1103/PhysRevA.95.013814)

I. INTRODUCTION

Emerging applications such as quantum information and low-power optical switching require strong interactions between single photons and quantum two-level systems (TLSs). One common technique to realize strong interactions is to confine photons in low dimensional spaces such as cavities or waveguides [1–3]. It leads to the tremendous success of cavity (waveguide) quantum electrodynamics [2,4–10]. On the other hand, it has been more difficult to achieve strong interactions in free space [11,12]. In the three-dimensional (3D) free space, the interaction can be characterized by the optical cross section [13–17]. The larger the cross section is, the easier it is for a photon to couple to the TLS [18,19]. However, it can be easily shown that the maximum cross section of a TLS with an electric dipole transition is $\sigma_d = 3\lambda^2/2\pi$ with λ being the transition wavelength [13,15,20]. The small size limits effective coupling in free space.

Large cross sections have been pursued for decades in the field of radio-frequency (rf) communication [17,20–22]. The goal is for a small circuit to capture free-space electromagnetic waves of an area as large as possible. The concept of a rf antenna introduces a key idea: the cross section can be enhanced by directional radiation [23–25]. The directivity of an antenna is defined by the normalized radiation pattern $D(\theta, \phi) = 4\pi U(\theta, \phi) / \iint U(\theta, \phi) d\Omega$, where $U(\theta, \phi)$ is the antenna's power radiated to the direction of the polar θ and the azimuthal ϕ angles. Classical antenna theory [26] shows that the maximum cross section σ_{\max} is directly related to the maximum directivity $D_{\max} \equiv \max[D(\theta, \phi)]$ by

$$\sigma_{\max} = \frac{\lambda^2}{\pi} D_{\max}. \quad (1)$$

For an isotropic antenna, $D_{\max} = 1$ and the maximum cross section is $\sigma_0 = \lambda^2/\pi$. A dipole antenna has zero emission along the axial direction of the dipole and thus has a higher directivity of $D_{\max} = 3/2$ [Fig. 1(a)] [26]. Consequently, its maximum cross section is slightly enhanced to $3\sigma_0/2$. In practice, sophisticated antennas [27–32] are designed to further enhance the directivity, such as the Yagi-Uda antenna [33–35] shown in Fig. 1(b). It emits more strongly in one direction

than the others. The maximum cross section can be further enhanced by several times than the dipole antenna.

Here we show that theorems and techniques developed in a classical antenna [36–39] are equally effective in a quantum antenna. A quantum antenna can be as simple as a single TLS as shown in Fig. 1(c), or a complex cluster of TLSs as shown in Fig. 1(d). Enhanced directivity allows quantum antennas to gain cross section as well as the coherence time, often orders of magnitude larger than those of a single TLS. Most importantly, all the enhancement is realized in free space. Large cross sections combined with long coherence time could be used for efficient interfacing of flying and stationary qubits in a free-space network.

II. QUANTUM SCATTERING THEORY

We start by using quantum scattering theory to prove Eq. (1) for a quantum antenna. The antenna is represented by a nondegenerate resonance with a ground state $|g\rangle$ and an excited state $|e\rangle$. These states can be realized in single atoms, quantum dots, or in complex systems such as the collective excitation states [40–42] in a cluster of atoms and quantum dots. The antenna's full Hamiltonian [43] can be cast as

$$H = \hbar\omega_0\sigma^\dagger\sigma + \sum_{\mathbf{k}} \hbar\omega_{\mathbf{k}}c_{\mathbf{k}}^\dagger c_{\mathbf{k}} + H_I. \quad (2)$$

The first two terms are the free Hamiltonians of the antenna and photons, respectively. Here $\sigma^\dagger = |e\rangle\langle g|$ and $\sigma = |g\rangle\langle e|$ are the usual raising and lowering atomic operators. The creation (annihilation) operator for photons is $c_{\mathbf{k}}^\dagger$ ($c_{\mathbf{k}}$). $\omega_{\mathbf{k}}$ and \mathbf{k} are the angular frequency and the wave vector, respectively. \hbar is the reduced Planck constant. The third term, H_I , describes the photon-antenna interaction, the specific form of which is not needed for proving Eq. (1).

The optical cross section can be calculated from a scattering process. The initial state is $|g, \mathbf{k}_i\rangle$, with the antenna in its ground state g and a single photon incident from a particular direction $\mathbf{k}_i(\theta_i, \phi_i)$. During the transient process of photon-antenna interaction, the antenna is partially excited while generating emission at the same time. After the interaction, the antenna eventually relaxes back to the ground state and the photon is scattered to many directions, represented by the final state $|g, \mathbf{k}_f\rangle$.

*zyu54@wisc.edu

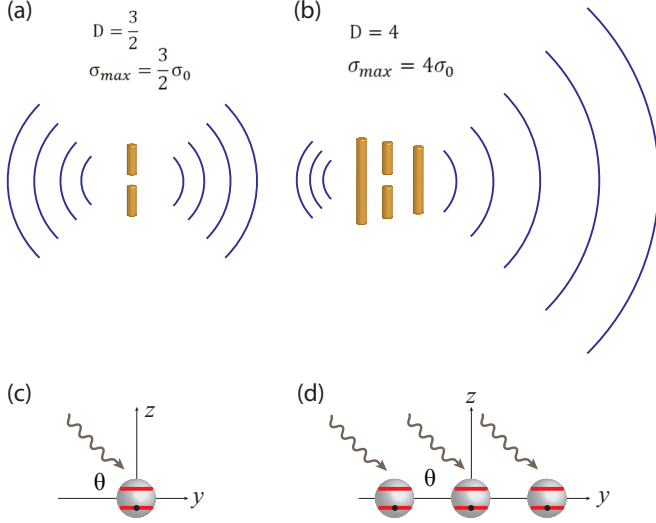


FIG. 1. (a) A classical dipole antenna made of metallic rods. (b) A Yagi-Uda antenna with three elements. The cross section increases as a result of the increased directivity of the radiation pattern. (c) The simplest quantum antenna is a TLS in the free space. (d) Three TLSs form an antenna with enhanced directivity and cross section.

The details of our quantum scattering theory are available in Appendix A. Unlike many approaches that treat the incident light as a semiclassical field [44], we use Fock states as the basis to solve the transport properties of light scattered by a cluster of TLSs in free space. A nonperturbative method [45] is adopted from waveguide quantum electrodynamics [46–49] to calculate the exact eigenstates of the open system, from which the scattering matrix and the cross sections can be obtained. Based on this theory, we show that the cross section follows a conservation law:

$$\iint \sigma(\theta, \phi) d\Omega = 4\lambda^2. \quad (3)$$

It shows that the total optical cross section is fundamentally limited. But it also indicates that the cross section can be enhanced for certain directions if other directions can be suppressed. We can define the directivity of the cross section as $\mathbb{D}(\theta, \phi) = 4\pi\sigma(\theta, \phi) / \iint \sigma(\theta, \phi) d\Omega$. Then Eq. (3) can be written as $\sigma(\theta, \phi) = \frac{\lambda^2}{\pi} \mathbb{D}(\theta, \phi)$, which is almost identical to Eq. (1) except that the directivity in Eq. (1) is defined for the radiation pattern. In Appendix B, we prove that the directivity is the same for the radiation pattern, the cross section, and the differential cross section.

We can easily verify Eq. (1) by considering the directivity and cross section of a dipole-transition TLS. However, in order to illustrate Eq. (1) in complex quantum antennas, we will study a cluster of TLSs. An example of three identical TLSs spaced by 0.075λ is shown in Fig. 1(d). These TLSs are closely packed within a subwavelength space. The small spacing induces strong interactions, resulting in collective excitation that gives rise to complex directivity unattainable in a single TLS. We will explicitly calculate the directivity, cross section, and the lifetime in these quantum antennas. The results not only verify Eq. (1) but also illustrate important ways of enhancing the light-TLS interaction in free space.

The free Hamiltonian for three TLSs of the antenna is $\omega_0 \sum_{m=1}^3 \sigma_m^\dagger \sigma_m$. The interaction Hamiltonian is $H_I = i\hbar \sum_{m=1}^3 \sum_{\mathbf{k}} [V_{\mathbf{k}}(\mathbf{r}_m) c_{\mathbf{k}}^\dagger \sigma_m - V_{\mathbf{k}}^*(\mathbf{r}_m) c_{\mathbf{k}} \sigma_m^\dagger]$, where \mathbf{r}_m is the position of the m th TLS. We assumed dipole transitions for all TLSs and the coupling constant is given by $V_{\mathbf{k}}(\mathbf{r}_m) = \omega_0 \sqrt{1/(2\hbar\epsilon_0\omega_{\mathbf{k}}L^3)} \mathbf{d}_m \cdot \mathbf{e}_{\mathbf{k}} u_{\mathbf{k}}(\mathbf{r}_m)$, where $u_{\mathbf{k}}(\mathbf{r}_m) = e^{i\mathbf{k}\cdot\mathbf{r}_m}$ and $\mathbf{e}_{\mathbf{k}}$ is the phase and unit polarization vector of the electric field of the wave. We have incorporated the polarizations in the \mathbf{k} summation. L^3 is the normalization volume.

In order to solve the Hamiltonian, we use the scattering theory developed in waveguide quantum electrodynamics [46,47] where the Hamiltonian is converted to a real-space representation. The boundary condition of this open system is specified by the condition of the incident photon and the eigenstates can be explicitly expressed. Here we further develop this approach for three-dimensional free space. The eigenstate can be written as the summation of photon wave functions in different directions as $|\phi\rangle = (\sum_{\mathbf{k}_i} \int d\xi \phi_{\mathbf{k}_i}(\xi) c_{\mathbf{k}_i}^\dagger(\xi) + \sum_{m=1}^3 e_m \sigma_m^\dagger) |0, g_1, g_2, g_3\rangle$, where e_m is the excitation amplitude of the m th TLS. $\phi_{\mathbf{k}_i}(\xi)$ is the wave function of the photon in the direction specified by \mathbf{k}_i with ξ being the spatial coordinate along the direction. $c_{\mathbf{k}_i}^\dagger(\xi)$ is the spatial creation operator of a propagating photon at position ξ in the direction \mathbf{k}_i . In Appendix A, we show how to use the time-independent Schrödinger equation to solve this scattering problem, from which we can obtain the scattering matrix, photon's wave functions, TLSs' excitation amplitudes e_m , and the cross section.

III. ENHANCEMENT OF CROSS SECTION AND LIFETIME

Figure 2(a) shows the spectrum of the cross section of the 3-TLS antenna when single photons are incident from the $\theta = 0^\circ$ direction. It shows three collective modes with resonant frequencies shifted away from ω_0 . The linewidths are also quite different from the natural bandwidth Γ_0 . This spectrum strongly depends on the incident angle θ : when $\theta = 90^\circ$, the central peak completely disappears [Fig. 2(b)]. The angular dependence of the cross section is displayed in Fig. 2(c). Three stripes can be identified, corresponding to three collective modes. In Fig. 7, we draw the relation between the spherical angles and the dipole moment.

The broadest mode, labeled by A in Fig. 2, is the superradiant mode [50–52]. Its spectral bandwidth is about three times the natural linewidth $\Gamma = 2.78\Gamma_0$. Since all three TLSs oscillate in phase with nearly equal amplitudes $e_1 \approx e_2 \approx e_3$ [Fig. 2(d)], the directivity $\mathbb{D}(\theta, \phi)$ of the superradiant mode closely resembles that of a single TLS, i.e., the donut-shape directivity, as shown in Fig. 2(d). The maximum directivity of $D_{\max} = 1.6$ and the maximum cross section of $\sigma_{\max} = 1.6\lambda^2/\pi$ exactly follow the relation dictated by Eq. (1). As limited by its dipolar directivity, the superradiant mode could not significantly enhance the cross section, regardless of the number of TLSs in the cluster.

In contrast to the superradiant mode A, the directivities of modes B and C are drastically different from the donut shape of a dipolar transition [second and third rows in Fig. 2(d)]. A maximum directivity of $D_{\max} = 3.6$ is observed in mode B.

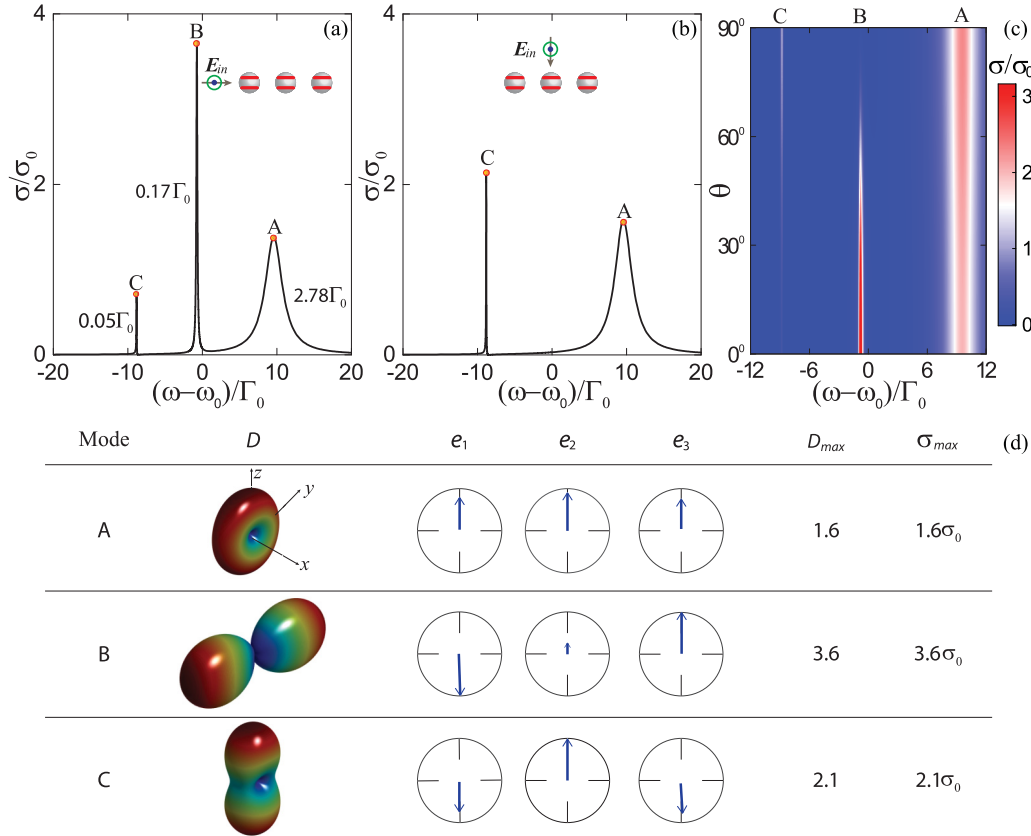


FIG. 2. The cross section of the photon incident angles with (a) $\theta = 0$ and (b) $\theta = 90$. (c) The cross-section spectra for incident angles from 0 to 90. (d) The cross section $\sigma(\theta, \phi)$ and directivities of three collective modes. The central column shows the complex excitation amplitudes of the constituent TLSs. The relative magnitude and phase of the complex excitation amplitudes e_i are represented by the length and the direction of the blue arrows.

The increased directivity is caused by the out-of-phase oscillation of three TLSs, whose amplitudes are displayed in Fig. 2(d). Destructive interference occurs for radiation in most directions, resulting in highly directional radiation. Strong directivity directly leads to an enhanced cross section of $\sigma_{max} = 3.6\lambda^2/\pi$.

Modes B and C are also referred to as the subradiant modes [50] because the destructive interference significantly decreases the spontaneous emission rates. Consequently, the lifetime is greatly enhanced. For example, a 20-fold enhancement of the lifetime is observed in mode C as shown by the bandwidth narrowing in Fig. 2(a). The longest lifetime generally increases with the number of TLSs in a quantum antenna. An example of a 5-TLS antenna to be shown later has a lifetime enhanced by 1143 times. Such superlong lifetime could provide long coherent storage of qubits [53–56].

From the analysis of the collective modes, we see that the coupling among TLSs plays a key role for enhancing directivity. A single factor that has the strongest effect on the coupling is the inter-TLS distance d . On one hand, d must be smaller than the wavelength to ensure adequate radiative coupling, a prerequisite for collective modes. On the other hand, when d is too small, radiative coupling becomes too strong such that it splits the energies of collective modes. The result is only moderate enhancement at three different frequencies.

Figure 3(a) shows the effect of d on cross-section spectra. At a deep subwavelength $d < 0.1\lambda$, three collective modes

split far apart, as shown by three dark stripes. Each only has a moderately enhanced cross section in the range of $1.5\sigma_0 < \sigma_{max} < 4\sigma_0$. On the other hand, at a large distance $d \gg \lambda$ [label ① in Fig. 3(a)], the lack of the radiative coupling makes the TLSs independent of each other. The directivity returns to a donut shape as shown in Fig. 3(b). The maximum cross section converges to a constant of $3 \times 1.5\sigma_0$, which is simply the incoherent addition of three independent dipolar TLSs [Fig. 3(c)].

An optimal antenna realizes the highest cross section when three collective modes just start to merge. It occurs when the inter-TLS distance d is around 0.2λ , as labeled by ② in Fig. 3(a). This distance strikes the optimal balance: the radiative coupling is strong enough to induce collective excitations but not so strong as to split resonant frequencies far apart. The maximum cross section reaches $\sigma_{max} = 9\sigma_0$ with a directivity drastically different from the donut shape [Fig. 3(b)].

In a similar way, the inter-TLS distance also has a dominant effect on the lifetime of the modes in quantum antennas. Figure 3(d) shows the lifetime of the collective mode with largest cross section. A lifetime of $73\tau_0$ is observed at $d = 0.14\lambda$. The lifetime quickly converges to the natural lifetime τ_0 when the distance increases as shown in Fig. 3(d).

Lastly, we discuss another way commonly used to increase the directivity of classical antennas: increasing the number of emission elements. Figure 4 shows the cross section and coherent time of antennas consisting of a linear array of N identical

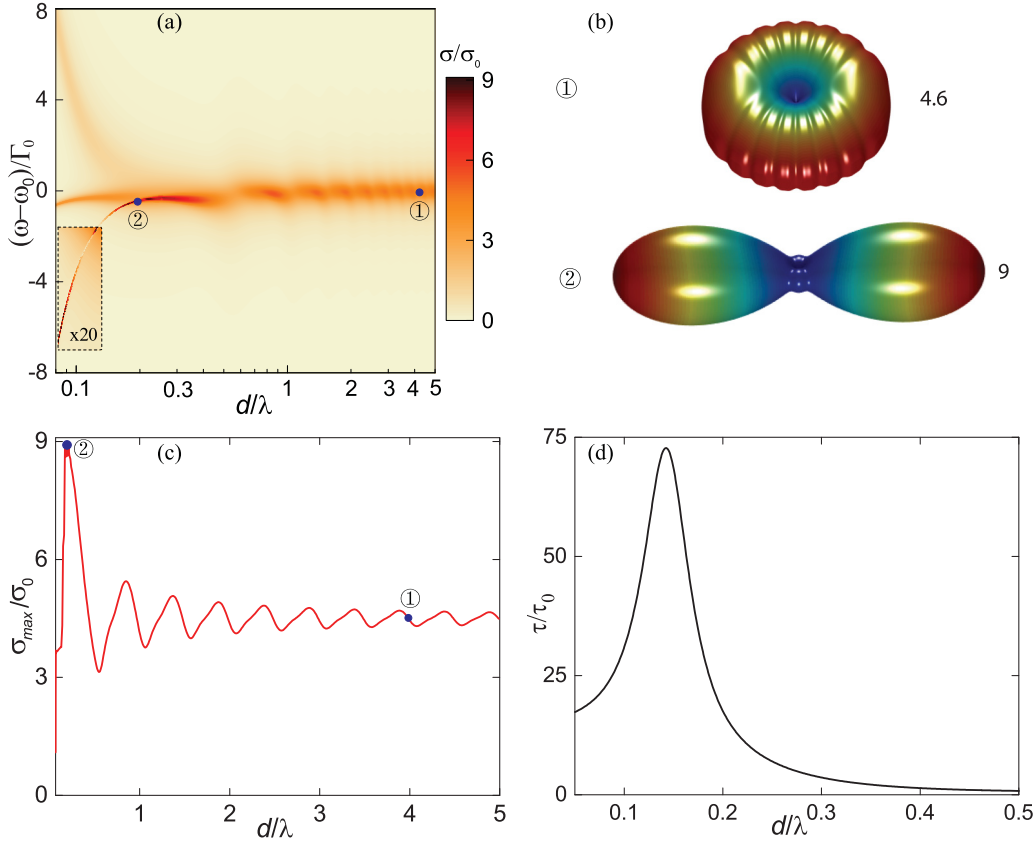


FIG. 3. (a) The cross-section spectra for different inter-TLS spacing d . The incident angle is $\theta = 0$. The values in the dashed box are multiplied by 20 times for easy visualization. (b) The cross sections $\sigma(\theta, \phi)$ for inter-TLS distances of 0.2λ and 4λ , respectively. (c) The maximum cross section σ_{\max} at different inter-TLS spacing d . It converges to the incoherent addition of $4.5\sigma_0$ when $d \gg \lambda$. (d) The lifetime of mode C as a function of the inter-TLS distance d .

TLs. For each antenna, an optimized inter-TLS distance d is used, which all happen to be around $0.2\lambda(1 \pm 5\%)$. Indeed, the maximum cross section increases as N increases, with a superlinear scaling. It reaches $\sigma_{\max} = 22.8\sigma_0$ for $N = 5$. In comparison, the dashed line shows the incoherent addition of N independent TLs, i.e., $N \times 1.5\sigma_0$. Quantum antennas perform far better than N independent TLs. The insets of Fig. 4(a) show the cross section $\sigma(\theta, \phi)$ for $N = 4$ and 5.

The maximum lifetime also increases with N as shown in Fig. 4(b). It becomes remarkably long, $\tau = 1143\tau_0$ when $N = 5$.

Scattering cross section describes a quantum antenna's capability in transferring photons from one far field to another. In practice, one might also want to transfer free-space photons to certain localized energy. The cross section for such transfer process can be easily calculated from the maximum scattering

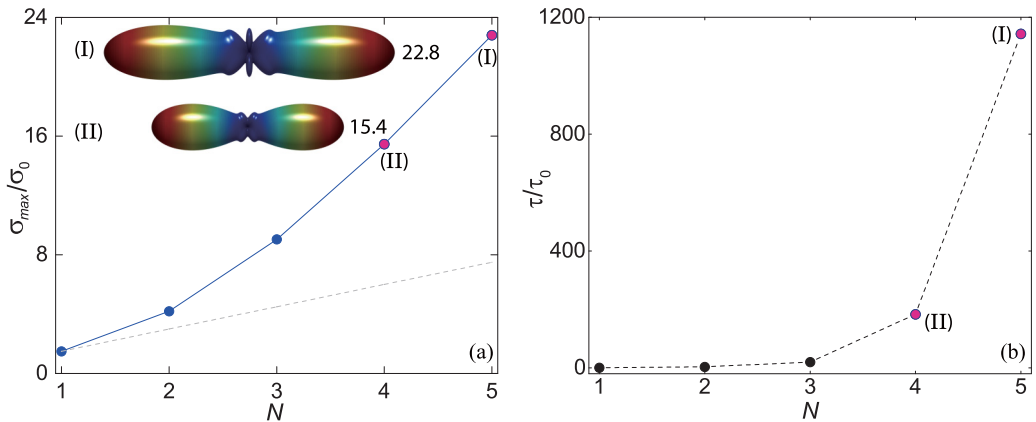


FIG. 4. (a) The maximum cross section of a quantum antenna increases with the number of TLs. The insets show $\sigma(\theta, \phi)$ for 4-TLS and 5-TLS antennas (marked with red dots), respectively. (b) The maximum coherent time also increases with N , reaching over 1000 times of natural lifetime τ_0 .

cross section, the rates of energy transfer to the localized energy, and radiation [57].

IV. CONCLUSIONS

In conclusion, directional quantum antennas greatly enhance the optical cross section and lifetime of TLSs in free space. Here we only showed the operation for single photons. It would certainly be interesting to extend the theory for multiphoton cases. Mediated by TLS's fermionic excitation, quantum antennas could induce strong photon-photon interactions, which can be useful for receiving and transmitting entanglement in free space. These efficient and yet compact receivers and transmitters could provide a scalable approach to construct a quantum information network in free space.

ACKNOWLEDGMENTS

This research is supported by the National Science Foundation (NSF) (Grants No. ECCS1405201 and No. ECCS1641006) and the National Natural Science Foundation of China (NSFC) (Grants No. 11334015, No. 11504115, and No. 11474114).

APPENDIX A: QUANTUM SCATTERING THEORY FOR MULTIPLE TLSs

Here we discuss the theoretical framework that we developed to solve the scattering problem of Fock-state photons scattered by multiple TLSs in free space. It is used to derive most of the analytical and numerical results shown in the main text. It uses a nonperturbative method to solve the scattering problem. Specifically, we solve the eigenstate of the full Hamiltonian, an open system that includes both TLSs and free-space photons. It treats incident light as a Fock state instead of semiclassical electric fields that drive the master equation. A similar approach has been developed in one-dimensional space in waveguide quantum electrodynamics (waveguide QED) [47,58,59]. The theory here works in 3D free space.

We consider a cluster of M TLSs in free space. The TLSs' excited states are $|e\rangle_{l=1,\dots,M}$; the ground states are $|g\rangle_{l=1,\dots,M}$; the transition frequencies are $\omega_{l=1,\dots,M}$; and transition dipole moments are $\mathbf{d}_{l=1,\dots,M}$. The TLSs are located at position $\xi_{l=1,\dots,M}$. With the electric dipole and rotating wave approximation, the Hamiltonian of the system with rotation-wave approximation (RWA) can be written as

$$H = \sum_{m=1}^M \hbar\omega_m \sigma_m^\dagger \sigma_m + \sum_k \hbar\omega_k c_k^\dagger c_k + i\hbar \sum_{m=1}^M \sum_k [V_k^*(\xi_m) c_k^\dagger \sigma_m - V_k(\xi_m) c_k \sigma_m^\dagger], \quad (\text{A1})$$

where ω_k is the angular frequency of the incident photon with a wave vector of \mathbf{k} . \hbar is the reduced Planck constant. c_k^\dagger and c_k are the bosonic creation and annihilation operator of the photon, respectively. σ_m^\dagger and σ_m are the raising and lowering atomic operators of the atoms, respectively. $V_k(\xi_m)$ is the coupling constant between the m th TLS and photons with a wave vector of \mathbf{k} .

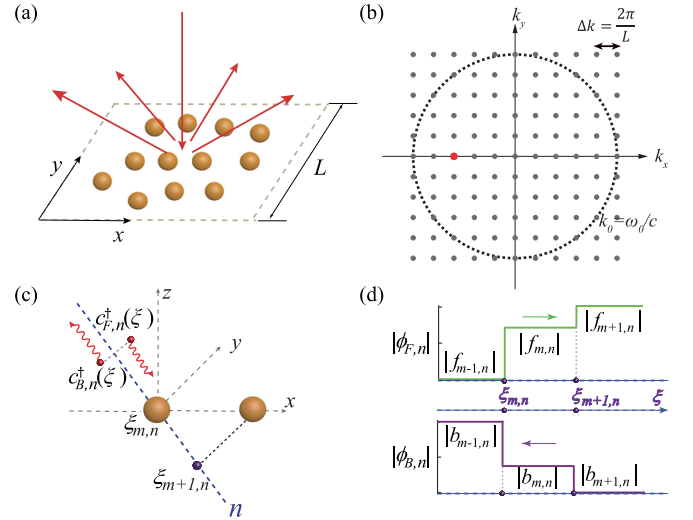


FIG. 5. (a) Schematic of a cluster of TLSs in free space. (b) Distribution of channels in the \mathbf{k}_{xy} space. The channels are discretized by $\Delta k = 2\pi/L$. The allowed channels are located within the circle with a radius of k_0 . (c) Real-space bosonic creation operators. $c_{F/B,n}^\dagger(\xi)$ creates a forward- or backward-moving photon at the location ξ in the n th channel. (d) Spatial single-photon wave functions in the n th channel. The coefficients are the amplitudes of forward (green line) and backward (purple line) directions between the m th and $(m+1)$ th TLSs in the n th channel, respectively.

We will explicitly solve for the eigenstates of the full Hamiltonian of the open system described by Eq. (A1). For this purpose, we need to do some preparation to transform the Hamiltonian into a real-space representation.

Free-space channels. First, we introduce the method to describe the continuum radiation in 3D free space. We will discretize the space by using the box quantization in a periodic boundary condition in the x - y plane [Fig. 5(a)]. The period is L . At the end of the derivation, we will take the limit of $L \rightarrow \infty$ to recover the case of free space. Because of the periodicity, an incident photon can only be scattered to a set of discrete directions. These directions are defined by the waves' in-plane wave vectors $\mathbf{k}_{xy} = (m_x, m_y)2\pi/L$, where m_x and m_y are integers [Fig. 5(b)]. We call these directions channels. As a convention of notation, the index (m_x, m_y) in the upper semi-infinite space also includes the waves in lower semi-infinite space in the direction of $(-m_x, -m_y)2\pi/L$. Channels are all located within the circle of $k_0 = \omega_0/c$ for the interested frequency range around the resonant frequency ω_0 . The total number is $N = \pi [L/\lambda_0]^2$, where $\lambda_0 = 2\pi/k_0$ is the resonant wavelength. The floor operator $[A]$ gives the largest integer smaller than A . Using channels, we can convert the Hamiltonian to

$$H = \sum_{m=1}^M \hbar\omega_m \sigma_m^\dagger \sigma_m + \sum_{n=1}^N \sum_k \hbar\omega_k c_{n,k}^\dagger c_{n,k} + i\hbar \sum_{m=1}^M \sum_{n=1}^N \sum_k [V_k^*(\xi_{m,n}) c_{n,k}^\dagger \sigma_m - V_k(\xi_{m,n}) c_{n,k} \sigma_m^\dagger]. \quad (\text{A2})$$

Here $\xi_{m,n}$ is the projected position of the m th TLS along the direction of the n th channel. The coupling coefficient $V_k(\xi_{m,n})$ is given by $V_k(\xi_{m,n}) = \omega_m \sqrt{1/2\hbar\varepsilon_0\omega_k L^3} \mathbf{d}_m \cdot \mathbf{e}_n e^{ik\xi_{m,n}}$, where ε_0 is vacuum permittivity, and \mathbf{e}_n is the polarization direction of the electric field of photons. By using $\sum_k = \Delta k \int dk$, we convert the Hamiltonian to

$$H = \sum_{m=1}^M \hbar\omega_m \sigma_m^\dagger \sigma_m + \sum_{n=1}^N \int dk \hbar\omega(k) c_n^\dagger(k) c_n(k) + i\hbar \sum_{m=1}^M \sum_{n=1}^N \int dk \sqrt{\frac{L}{2\pi}} [V_{m,n}(k) e^{-ik\xi_{m,n}} c_n^\dagger(k) \sigma_m - V_{m,n}(k) e^{ik\xi_{m,n}} c_n(k) \sigma_m^\dagger], \quad (\text{A3})$$

where $c_n^\dagger(k) = \sqrt{L/2\pi} c_{n,k}^\dagger$ and $c_n(k) = \sqrt{L/2\pi} c_{n,k}$. $V_{m,n}(k) = \omega_m \sqrt{1/2\hbar\varepsilon_0\omega_k L^3} \mathbf{d}_m \cdot \mathbf{e}_n$. By further defining $\tilde{V}_{m,n} = V_{m,n}(k) \sqrt{L/2\pi}$, we can simplify Eq. (A3) to

$$H = \sum_{m=1}^M \hbar\omega_m \sigma_m^\dagger \sigma_m + \sum_{n=1}^N \int dk \hbar\omega(k) c_n^\dagger(k) c_n(k) + i\hbar \sum_{m=1}^M \sum_{n=1}^N \int dk \tilde{V}_{m,n} [c_n^\dagger(k) e^{-ik\xi_{m,n}} \sigma_m - c_n(k) e^{ik\xi_{m,n}} \sigma_m^\dagger]. \quad (\text{A4})$$

There are two propagation directions in each channel, i.e., the forward and backward-propagation directions. Thus, we can express the second term on the right-hand side in Eq. (A4) as

$$\sum_{n=1}^N \int dk \hbar\omega(k) c_n^\dagger(k) c_n(k) = \sum_{n=1}^N \int dk \hbar\omega(k) c_{F,n}^\dagger(k) c_{F,n}(k) + \sum_{n=1}^N \int dk \hbar\omega(k) c_{B,n}^\dagger(k) c_{B,n}(k), \quad (\text{A5})$$

and the last term as

$$\begin{aligned} & i\hbar \sum_{m=1}^M \sum_{n=1}^N \int dk \tilde{V}_{m,n} [c_n^\dagger(k) e^{-ik\xi_{m,n}} \sigma_m - c_n(k) e^{ik\xi_{m,n}} \sigma_m^\dagger] \\ &= i\hbar \sum_{m=1}^M \sum_{n=1}^N \int dk \tilde{V}_{m,n} \{ [c_{F,n}^\dagger(k) + c_{B,n}^\dagger(k)] e^{-ik\xi_{m,n}} \sigma_m - [c_{F,n}(k) + c_{B,n}(k)] e^{ik\xi_{m,n}} \sigma_m^\dagger \}. \end{aligned} \quad (\text{A6})$$

Convert to real-space Hamiltonian. Now that we have expressed the free-space radiation in terms of channels, we begin to convert the Hamiltonian to a real-space representation. Each channel is effectively a one-directional waveguide, which allows us to apply an important technique developed in waveguide QED [46]. Specifically, we will convert the k -space operators $c_{F,n}^\dagger(k), c_{B,n}^\dagger(k), c_{F,n}(k)$, and $c_{B,n}(k)$ to real-space operators by applying the following Fourier transformation [46]:

$$c_{F/B,n}^\dagger(k) = \frac{1}{\sqrt{2\pi}} \int_{-\infty}^{\infty} c_{F/B,n}^\dagger(\xi) e^{ik\xi} d\xi, \quad (\text{A7a})$$

$$c_{F/B,n}(k) = \frac{1}{\sqrt{2\pi}} \int_{-\infty}^{\infty} c_{F/B,n}(\xi) e^{-ik\xi} d\xi, \quad (\text{A7b})$$

where $c_{F/B,n}^\dagger(\xi)$ and $c_{F/B,n}(\xi)$ [illustrated in Fig. 5(c)] create and annihilate a forward- and backward-propagation photon at position ξ in the n th channel, respectively. Using the above Fourier transformation, the Hamiltonian can be expressed in real space as

$$\begin{aligned} H &= \sum_{m=1}^M \hbar\omega_m \sigma_m^\dagger \sigma_m + \sum_{n=1}^N \int_{-\infty}^{\infty} d\xi (-i\hbar c) \left[c_{F,n}^\dagger(\xi) \frac{d}{d\xi} c_{F,n}(\xi) - c_{B,n}^\dagger(\xi) \frac{d}{d\xi} c_{B,n}(\xi) \right] \\ &+ i\hbar \sum_{m=1}^M \sum_{n=1}^N \int_{-\infty}^{\infty} d\xi \delta(\xi - \xi_{m,n}) V_{m,n} \{ [c_{F,n}^\dagger(\xi) + c_{B,n}^\dagger(\xi)] \sigma_m - [c_{F,n}(\xi) + c_{B,n}(\xi)] \sigma_m^\dagger \}, \end{aligned} \quad (\text{A8})$$

where $\xi_{m,n}$ is the projected location of the m th TLS in the n th channel. Here we have used the dispersion relation $\omega(k) = ck$ and $\omega(k) = -ck$ for the forward- and backward-propagating waves, respectively. The coupling constant is $V_{m,n} = \sqrt{2\pi} \tilde{V}_{m,n}$.

Eigenstates of real-space Hamiltonian. The general form of the eigenstates of Eq. (A8) is given by

$$|\phi\rangle = \left\{ \sum_{n=1}^N \int d\xi [\phi_{F,n}(\xi) c_{F,n}^\dagger(\xi) + \phi_{B,n}(\xi) c_{B,n}^\dagger(\xi)] + \sum_{m=1}^M e_m \sigma_m^\dagger \right\} |0, g_1, \dots, g_M\rangle. \quad (\text{A9})$$

Here we only consider the single-photon case. $\phi_{F,n}(\xi)$ and $\phi_{B,n}(\xi)$ are the spatial wave functions of forward- and backward-propagating photons in the n th channel, respectively. $|0, g_1, \dots, g_M\rangle$ is the zero photon state with all the TLSs in the ground states. e_m is the excitation amplitude of the m th TLS. By solving the time-independent Schrödinger equation $H|\phi\rangle = E|\phi\rangle$,

where $E = \hbar\omega$ is the eigenenergy of the system, we get

$$-ic \frac{d}{d\xi} \phi_{F,n}(\xi) + i \sum_{m=1}^M V_{m,n} \delta(\xi - \xi_{m,n}) e_m = \omega \phi_{F,n}(\xi), \quad (\text{A10})$$

$$ic \frac{d}{d\xi} \phi_{B,n}(\xi) + i \sum_{m=1}^M V_{m,n} \delta(\xi - \xi_{m,n}) e_m = \omega \phi_{B,n}(\xi), \quad (\text{A11})$$

$$\omega_m e_m - i \sum_{n=1}^N V_{m,n} [\phi_{F,n}(\xi_{m,n}) + \phi_{B,n}(\xi_{m,n})] = \omega e_m. \quad (\text{A12})$$

To be specific, we consider a photon incident from the p th channel. The wave function in the n th channel can be written as

$$\phi_{F,n}(\xi) = e^{ik\xi} \left[\theta(\xi_{1,n} - \xi) \delta_{np} + \sum_{m=1}^{M-1} f_{m,n} \theta(\xi - \xi_{m,n}) \theta(\xi_{m+1,n} - \xi) + f_{M,n} \theta(\xi - \xi_{M,n}) \right], \quad (\text{A13})$$

$$\phi_{B,n}(\xi) = e^{-ik\xi} \left[b_{0,n} \theta(\xi_{1,n} - \xi) + \sum_{m=1}^{M-1} b_{m,n} \theta(\xi - \xi_{m,n}) \theta(\xi_{m+1,n} - \xi) \right]. \quad (\text{A14})$$

Here $\theta(\xi)$ is the step function and δ_{np} is the Kronecker delta. The coefficients $f_{m,n}$ and $b_{m,n}$ are the amplitudes of forward- and backward-propagating waves between the m th and $(m+1)$ th TLSs in the n th channel, respectively. They are schematically shown in Fig. 5(d).

Substituting Eq. (A13) into Eq. (A10), we can get

$$-ice^{ik\xi_{1,n}}(-\delta_{np} + f_{1,n}) + iV_{1,n}e_1 = 0, \quad (\text{A15a})$$

$$-ice^{ik\xi_{m,n}}(-f_{m-1,n} + f_{m,n}) + iV_{m,n}e_m = 0, \quad (\text{A15b})$$

$$-ice^{ik\xi_{M,n}}(-f_{M-1,n} + f_{M,n}) + iV_{M,n}e_M = 0. \quad (\text{A15c})$$

Substituting Eq. (A14) into Eq. (A11), we also can get

$$ice^{-ik\xi_{1,n}}(b_{1,n} - b_{0,n}) + iV_{1,n}e_1 = 0, \quad (\text{A16a})$$

$$ice^{-ik\xi_{m,n}}(b_{m,n} - b_{m-1,n}) + iV_{m,n}e_m = 0, \quad (\text{A16b})$$

$$ice^{-ik\xi_{M,n}}(-b_{M-1,n}) + iV_{M,n}e_M = 0. \quad (\text{A16c})$$

Next, we can directly solve Eq. (A15) and get the amplitudes of the forward-propagating waves

$$f_{1,n} = \frac{V_{1,n}}{c} e^{-ik\xi_{1,n}} e_1 + \delta_{np}, \quad (\text{A17a})$$

$$f_{m,n} = \frac{V_{m,n}}{c} e^{-ik\xi_{m,n}} e_m + \dots + \frac{V_{1,n}}{c} e^{-ik\xi_{1,n}} e_1 + \delta_{np}, \quad (\text{A17b})$$

$$f_{M,n} = \frac{V_{M,n}}{c} e^{-ik\xi_{M,n}} e_M + \dots + \frac{V_{1,n}}{c} e^{-ik\xi_{1,n}} e_1 + \delta_{np}. \quad (\text{A17c})$$

Similarly, we solve Eq. (A16) and get the amplitudes of backward-propagating waves

$$b_{0,n} = \frac{V_{M,n}}{c} e^{ik\xi_{M,n}} e_M + \dots + \frac{V_{m,n}}{c} e^{ik\xi_{m,n}} e_m + \dots + \frac{V_{1,n}}{c} e^{ik\xi_{1,n}} e_1, \quad (\text{A18a})$$

$$b_{m-1,n} = \frac{V_{M,n}}{c} e^{ik\xi_{M,n}} e_M + \dots + \frac{V_{m,n}}{c} e^{ik\xi_{m,n}} e_m, \quad (\text{A18b})$$

$$b_{M,n} = \frac{V_{M,n}}{c} e^{ik\xi_{M,n}} e_M. \quad (\text{A18c})$$

Now, we use these results to calculate the summation in Eq. (A12) and get

$$\omega_m e_m - i \left(V_{m,p} e^{ik\xi_{m,p}} + \sum_{n=1}^N \frac{V_{m,n}^2}{2c} e_m + \sum_{l=1, l \neq m}^M \sum_{n=1}^N \frac{V_{m,n} V_{l,n}}{2c} e^{ik|\xi_{m,n} - \xi_{l,n}|} e_l \right) = \omega e_m. \quad (\text{A19})$$

Equation (A19) can be written in a more compact form. For this purpose, we define $\Gamma_{m,n} = \frac{V_{m,n}^2}{c}$ and $\Gamma_m = \sum_{n=1}^N \frac{V_{m,n}^2}{2c} = \sum_{n=1}^N \Gamma_{m,n}$. Γ_m is the spontaneous emission rate of the m th scatterer. Sum over all the channels; then Eq. (A20) can be written as

$$\left(\omega - \omega_m + i \frac{\Gamma_m}{2} \right) e_m + \sum_{l=1, l \neq m}^M \left(-\Xi_{ml} + i \frac{\Gamma_{ml}}{2} \right) e_l = -iV_{m,p} e^{ik\xi_{m,p}}. \quad (\text{A20})$$

Here we also use the collective spontaneous rate Γ_{ml} and the induced dipole-dipole interaction Ξ_{ml} arising from the coupling between the m th and the l th TLSs through the vacuum field [41,60]: $\Gamma_{ml} = \sqrt{\Gamma_m \Gamma_l} \frac{3}{2} F_{ml}(k\xi_{ml})$ and $\Xi_{ml} = \sqrt{\Gamma_m \Gamma_l} \frac{3}{4} Q_{ml}(k\xi_{ml})$, where $F_{ml}(k\xi_{ml}) = \sum_{n=1}^N \frac{e^{ik|\xi_{m,n} - \xi_{l,n}|}}{2} = [\mathbf{d}_m \cdot \mathbf{d}_l - (\mathbf{d}_m \cdot \hat{\mathbf{r}})(\mathbf{d}_l \cdot \hat{\mathbf{r}})] \frac{\sin(k\xi_{ml})}{k\xi_{ml}} + [\mathbf{d}_m \cdot \mathbf{d}_l - 3(\mathbf{d}_m \cdot \hat{\mathbf{r}})(\mathbf{d}_l \cdot \hat{\mathbf{r}})] \frac{\cos(k\xi_{ml})}{(k\xi_{ml})^2} - \frac{\sin(k\xi_{ml})}{(k\xi_{ml})^3}$, and $Q_{ml}(k\xi_{ml}) = -[\mathbf{d}_m \cdot \mathbf{d}_l - (\mathbf{d}_m \cdot \hat{\mathbf{r}})(\mathbf{d}_l \cdot \hat{\mathbf{r}})] \frac{\cos(k\xi_{ml})}{k\xi_{ml}} + [\mathbf{d}_m \cdot \mathbf{d}_l - 3(\mathbf{d}_m \cdot \hat{\mathbf{r}})(\mathbf{d}_l \cdot \hat{\mathbf{r}})] \frac{\sin(k\xi_{ml})}{(k\xi_{ml})^2} + \frac{\cos(k\xi_{ml})}{(k\xi_{ml})^3}$. Here ξ_{ml} and $\hat{\mathbf{r}}$ are the distance and the unit vector between the m th and the l th TLSs, respectively.

Cross sections. Using Eqs. (A17c) and (A18a), we can derive the scattering cross section [61]

$$\sigma(\omega) = \frac{\sum_{n=1}^N (f_{M,n}^\dagger) f_{M,n} + \sum_{n=1}^N (b_{0,n}^\dagger) b_{0,n}}{1/L^2} = \frac{3\lambda^2}{2\pi} \left[\sum_{m=1}^M \frac{\Gamma_m}{2} |\tilde{e}_m|^2 + \sum_{m=1, m \neq l}^M \sum_{l=1}^M \frac{\Gamma_{ml}}{2} \tilde{e}_l^* \tilde{e}_m \right]. \quad (\text{A21})$$

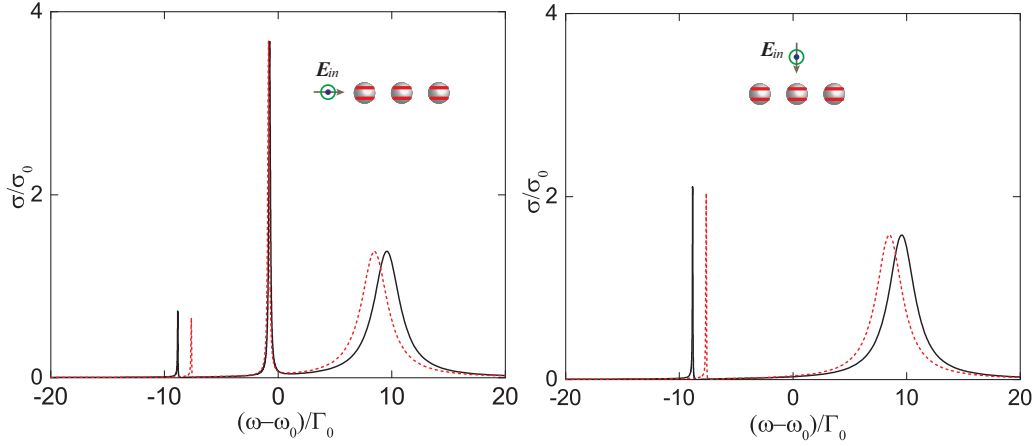


FIG. 6. The scattering cross section calculated with (red lines) and without (black solid lines) rotation-wave approximation for light incident from two different directions.

Here we use the relation $e_m = \sqrt{\frac{3\lambda^2}{2\pi} \frac{1}{2} \frac{1}{L} \tilde{e}_m}$. Analytical solutions for one and two TLSs can be directly derived [45]. But for more than two TLSs, we resort to the numerical calculation in the main text.

The rotation-wave approximation is applied in the interaction part of our quantum scattering theory in Eq. (A1). Here we also calculate the results without using rotation-wave approximation [62]. The results are shown by black solid curves in Fig. 6. Compared to the red curves obtained from RWA, the magnitudes of the cross sections are not affected significantly despite the slight frequency shift of the resonant peaks.

Conservation law. Here we prove that the total cross section of a single nondegenerate TLS is fundamentally constrained, regardless of the specific implementation of the resonance.

The Hamiltonian H of the system under study can be written as two parts,

$$H = H_0 + H_I, \quad (\text{A22})$$

where $H_0 = \hbar\omega_0\sigma^\dagger\sigma + \sum_k \hbar\omega_k c_k^\dagger c_k$ is the free Hamiltonian of the TLSs and photons, and H_I is the interaction between them. Here, we consider the initial and final states of the scattering process are eigenstates of the free Hamiltonian. For scattering of single photons, the initial state and final state of the scattering process are represented by $|g, \mathbf{k}_i\rangle$ and $|g, \mathbf{k}_f\rangle$, respectively.

The scattering cross section is given by $\sigma = \frac{\sum_{\mathbf{k}_f} T_{fi}}{\Phi}$, where $\Phi = \frac{c}{L^3}$ is the density of photon flux and $T_{fi} = \frac{2\pi}{\hbar} |\mathfrak{S}_{fi}|^2 \delta(\hbar\omega_{\mathbf{k}_f} - \hbar\omega_{\mathbf{k}_i})$ is the transition rate from the initial state to the final state [44]. Here \mathfrak{S}_{fi} is the transition matrix. The period L , which is larger than the wavelength, is used for normalization purposes. In general, we consider the resonant scattering, i.e., the incident photon frequency $\omega_{\mathbf{k}_i}$ equals the transition frequency ω_0 of the TLS.

The transition matrix can be obtained from the time evolution of the system [63], which can be written as

$$\mathfrak{S}_{fi} = \frac{\langle g, \mathbf{k}_f | H_I | e, 0 \rangle \langle e, 0 | H_I | g, \mathbf{k}_i \rangle}{\hbar\omega - \hbar\omega_0 - \hbar\Delta + i\pi \sum_{\mathbf{k}_f} |\langle g, \mathbf{k}_f | H_I | e, 0 \rangle|^2 \delta(\hbar\omega_{\mathbf{k}_f} - \hbar\omega_0)}, \quad (\text{A23})$$

where $\Delta = \frac{1}{\hbar} \wp \sum_{\mathbf{k}_f} \frac{|\langle g, \mathbf{k}_f | H_I | e, 0 \rangle|^2}{\hbar\omega_0 - \hbar\omega_{\mathbf{k}_f}}$ is the frequency shift and \wp indicates the Cauchy principal value. The transition matrix element \mathfrak{S}_{fi} is a complex number which exhibits a resonance for $\omega = \omega_0 + \Delta$. At resonance, \mathfrak{S}_{fi} is purely imaginary and its amplitude is maximal.

The scattering cross section now can be written as

$$\sigma(\theta_i, \phi_i) = \frac{2L^3}{\hbar c} \frac{\pi \sum_{\mathbf{k}_f} |\langle g, \mathbf{k}_f | H_I | e, 0 \rangle \langle e, 0 | H_I | g, \mathbf{k}_i \rangle|^2 \delta(\hbar\omega_{\mathbf{k}_f} - \hbar\omega_0)}{(\hbar\omega - \hbar\omega_0 - \hbar\Delta)^2 + [\pi \sum_{\mathbf{k}_f} |\langle g, \mathbf{k}_f | H_I | e, 0 \rangle|^2 \delta(\hbar\omega_{\mathbf{k}_f} - \hbar\omega_0)]^2}. \quad (\text{A24})$$

We can further simplify Eq. (A24) to

$$\sigma(\theta_i, \phi_i) = \frac{2L^3}{\pi \hbar c} \frac{[|\langle e, 0 | H_I | g, \mathbf{k}_i \rangle|^2]}{[\sum_{\mathbf{k}_f} |\langle g, \mathbf{k}_f | H_I | e, 0 \rangle|^2 \delta(\hbar\omega_{\mathbf{k}_f} - \hbar\omega_0)]} \frac{[\pi \sum_{\mathbf{k}_f} |\langle g, \mathbf{k}_f | H_I | e, 0 \rangle|^2 \delta(\hbar\omega_{\mathbf{k}_f} - \hbar\omega_0)]^2}{(\hbar\omega - \hbar\omega_0 - \hbar\Delta)^2 + [\pi \sum_{\mathbf{k}_f} |\langle g, \mathbf{k}_f | H_I | e, 0 \rangle|^2 \delta(\hbar\omega_{\mathbf{k}_f} - \hbar\omega_0)]^2}. \quad (\text{A25})$$

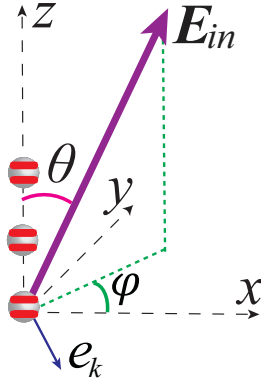


FIG. 7. The TLs arrangement along the z axis and the dipole moment \mathbf{d} along the x axis. \mathbf{e}_k is the polarization of the incident direction and is perpendicular to the incident direction. θ and φ are the polar and azimuthal angles of the incident photon.

At the resonance scattering peak for $\omega = \omega_0 + \Delta$, the cross section is

$$\sigma(\theta_i, \phi_i) = \frac{2L^3}{\hbar\pi c} \frac{\pi |\langle e, 0 | H_I | g, \mathbf{k}_i \rangle|^2}{\sum_{\mathbf{k}_f} |\langle g, \mathbf{k}_f | H_I | e, 0 \rangle|^2 \delta(\hbar\omega_{\mathbf{k}_f} - \hbar\omega_0)}. \quad (\text{A26})$$

The denominator summation over the scattered state in Eq. (A26) can be converted into an integration over frequency and solid angle $d\Omega$ by the relation $\sum_{\mathbf{k}_f} \rightarrow \frac{L^3}{(2\pi)^3} \int \frac{\omega^2}{\hbar c^3} d\omega d\Omega$. Integrating Eq. (A26) over the 4π solid angle, we can easily get the integration as

$$\begin{aligned} \int \sigma(\theta_i, \phi_i) d\Omega &= \frac{2L^3}{\hbar\pi c} \frac{\pi \int |\langle e, 0 | H_I | g, \mathbf{k}_i \rangle|^2 d\Omega}{\int |\langle g, \mathbf{k}_f | H_I | e, 0 \rangle|^2 d\Omega \rho(\omega_0)} \\ &= \frac{2L^3}{\hbar\pi c \rho(\omega_0)}, \end{aligned} \quad (\text{A27})$$

where $\rho(\omega_0) = \frac{L^3}{(2\pi)^3} \frac{\omega_0^2}{\hbar c^3}$ is the density of the photon [63]. Therefore, the total cross section is given by

$$\int \sigma(\theta_i, \phi_i) d\Omega = 4\lambda_0^2. \quad (\text{A28})$$

Equation (A28) indicates the conservation law of total cross section. Note we do not need the specific form of H_I to obtain Eq. (A28). It holds true for any nondegenerate TLS.

APPENDIX B: THE DIRECTIVITY OF RADIATION, CROSS SECTION, AND DIFFERENTIAL CROSS SECTION

In this appendix, we prove that the directivities of the radiation pattern, cross section, and differential cross section are the same.

The radiation pattern can be obtained by considering the evolution of an excited state without incident photons, i.e., $|e, 0\rangle$. The power radiated to a direction (θ_i, ϕ_i) is related to the transition probability amplitude $\langle g, \mathbf{k}_i | H_I | e, 0 \rangle$. The directivity of the radiation pattern is given by

$$D(\theta_i, \phi_i) = 4\pi \frac{\langle g, \mathbf{k}_i | H_I | e, 0 \rangle \langle e, 0 | H_I | g, \mathbf{k}_i \rangle}{\sum_i \langle e, 0 | H_I | g, \mathbf{k}_i \rangle \langle g, \mathbf{k}_i | H_I | e, 0 \rangle}.$$

Here $|\mathbf{k}_i\rangle$ represents a photon in the direction of \mathbf{k}_i . The numerator is the probability of the excited state decaying to a photon in the direction \mathbf{k}_i . The denominator is the total probability of decaying to all directions.

The total cross section for a particular incident direction \mathbf{k}_i is proportional to the summation of the transition probability to all final states as $\sum_f |\langle g, \mathbf{k}_f | H_I | e, 0 \rangle \langle e, 0 | H_I | g, \mathbf{k}_i \rangle|^2$. Thus the directivity of the cross section can be calculated as

$$\mathbb{D}(\theta_i, \phi_i) = 4\pi \frac{\sum_f |\langle g, \mathbf{k}_f | H_I | e, 0 \rangle \langle e, 0 | H_I | g, \mathbf{k}_i \rangle|^2}{\sum_{f,i} |\langle g, \mathbf{k}_f | H_I | e, 0 \rangle \langle e, 0 | H_I | g, \mathbf{k}_i \rangle|^2},$$

where the denominator accounts for the summation over all incident directions. We can easily show that

$$\begin{aligned} \mathbb{D}(\theta_i, \phi_i) &= 4\pi \frac{\sum_f |\langle g, \mathbf{k}_f | H_I | e, 0 \rangle|^2 |\langle e, 0 | H_I | g, \mathbf{k}_i \rangle|^2}{\sum_f |\langle g, \mathbf{k}_f | H_I | e, 0 \rangle|^2 \sum_i |\langle e, 0 | H_I | g, \mathbf{k}_i \rangle|^2} \\ &= 4\pi \frac{|\langle e, 0 | H_I | g, \mathbf{k}_i \rangle|^2}{\sum_i |\langle e, 0 | H_I | g, \mathbf{k}_i \rangle|^2} = D. \end{aligned}$$

The directivity of the differential cross section can also be calculated from the transition probability as

$$\mathfrak{D}(\theta_i, \phi_i) = 4\pi \frac{|\langle g, \mathbf{k}_f | H_I | e, 0 \rangle \langle e, 0 | H_I | g, \mathbf{k}_i \rangle|^2}{\sum_f |\langle g, \mathbf{k}_f | H_I | e, 0 \rangle \langle e, 0 | H_I | g, \mathbf{k}_i \rangle|^2}.$$

We can further simplify as

$$\mathfrak{D}(\theta_i, \phi_i) = 4\pi \frac{|\langle e, 0 | H_I | g, \mathbf{k}_i \rangle|^2 |\langle g, \mathbf{k}_f | H_I | e, 0 \rangle|^2}{|\langle e, 0 | H_I | g, \mathbf{k}_i \rangle|^2 \sum_f |\langle g, \mathbf{k}_f | H_I | e, 0 \rangle|^2}$$

It is straightforward to verify that $D = \mathbb{D} = \mathfrak{D}$. The radiation pattern, cross section, and differential cross section have the same directivity.

APPENDIX C: DEFINITION OF THE ANGLES USED IN THE DERIVATION

The spectrum of the cross section shown in Figs. 2(a)–2(c) depends on the incident and polarization direction of the single photons. Without loss of generality, here we arrange the TLs along the z axis and define the dipole directions along the x -axis directions. θ and φ are the polar and azimuthal angles of the incident photon. \mathbf{e}_k is the polarization direction of the incident photon which is perpendicular to the incident direction. In Figs. 2(a)–2(c), we define $\varphi = 0$. The polarization of the incident photon is parallel with the dipole direction.

[1] C. J. Hood, T. W. Lynn, A. C. Doherty, A. S. Parkins, and H. J. Kimble, *Science* **287**, 1447 (2000).

[2] I. Söllner, S. Mahmoodian, S. L. Hansen, L. Midolo, A. Javadi, G. Kiršanskė, T. Pregolato, H. El-Ella, E. H. Lee, J. D. Song, S. Stobbe, and P. Lodahl, *Nat. Nanotechnol.* **10**, 775 (2015).

- [3] A. Goban, C. L. Hung, J. D. Hood, S. P. Yu, J. A. Muniz, O. Painter, and H. J. Kimble, *Phys. Rev. Lett.* **115**, 063601 (2015).
- [4] K. Hennessy, A. Badolato, M. Winger, D. Gerace, M. Atature, S. Gulde, S. Falt, E. L. Hu, and A. Imamoglu, *Nature (London)* **445**, 896 (2007).
- [5] M. Mücke, E. Figueroa, J. Bochmann, C. Hahn, K. Murr, S. Ritter, C. J. Villas-Boas, and G. Rempe, *Nature (London)* **465**, 755 (2010).
- [6] M. Harlander, R. Lechner, M. Brownnutt, R. Blatt, and W. Hansel, *Nature (London)* **471**, 200 (2011).
- [7] J. D. Thompson, T. G. Tiecke, N. P. de Leon, J. Feist, A. V. Akimov, M. Gullans, A. S. Zibrov, V. Vuletić, and M. D. Lukin, *Science* **340**, 1202 (2013).
- [8] J. S. Douglas, H. Habibian, C. L. Hung, A. V. Gorshkov, H. J. Kimble, and D. E. Chang, *Nat. Photonics* **9**, 326 (2015).
- [9] A. J. Bennett *et al.*, *Sci. Adv.* **2**, e1501256 (2016).
- [10] X. Ding *et al.*, *Phys. Rev. Lett.* **116**, 020401 (2016).
- [11] M. K. Tey, Z. Chen, S. A. Aljunid, B. Chng, F. Huber, G. Maslennikov, and C. Kurtsiefer, *Nat. Phys.* **4**, 924 (2008).
- [12] G. Hétet, L. Slodička, M. Hennrich, and R. Blatt, *Phys. Rev. Lett.* **107**, 133002 (2011).
- [13] G. Zumofen, N. M. Mojarad, V. Sandoghdar, and M. Agio, *Phys. Rev. Lett.* **101**, 180404 (2008).
- [14] K. Konthasinghe *et al.*, *Phys. Rev. B* **85**, 235315 (2012).
- [15] X. W. Chen, V. Sandoghdar, and M. Agio, *Phys. Rev. Lett.* **110**, 153605 (2013).
- [16] J. Pellegrino, R. Bourgain, S. Jennewein, Y. R. P. Sortais, A. Browaeys, S. D. Jenkins, and J. Ruostekoski, *Phys. Rev. Lett.* **113**, 133602 (2014).
- [17] R. J. Bettles, S. A. Gardiner, and C. S. Adams, *Phys. Rev. Lett.* **116**, 103602 (2016).
- [18] M. Scheibner, T. Schmidt, L. Worschech, A. Forchel, G. Bacher, T. Passow, and D. Hommel, *Nat. Phys.* **3**, 106 (2007).
- [19] R. Röhlberger, K. Schlage, B. Sahoo, S. Couet, and R. Ruffer, *Science* **328**, 1248 (2010).
- [20] M. Zhou, L. Shi, J. Zi, and Z. Yu, *Phys. Rev. Lett.* **115**, 023903 (2015).
- [21] L. Cao, J. S. White, J. S. Park, J. A. Schuller, B. M. Clemens, and M. L. Brongersma, *Nat. Mater.* **8**, 643 (2009).
- [22] T. Meng Khoon, M. Gleb, C. H. L. Timothy, A. Syed Abdullah, H. Florian, C. Brenda, C. Zilong, S. Valerio, and K. Christian, *New J. Phys.* **11**, 043011 (2009).
- [23] T. Coenen, F. Bernal Arango, A. Femius Koenderink, and A. Polman, *Nat. Commun.* **5**, 3250 (2014).
- [24] M. O. Scully, E. S. Fry, C. H. R. Ooi, and K. Wódkiewicz, *Phys. Rev. Lett.* **96**, 010501 (2006).
- [25] Y. Miroshnichenko, U. V. Poulsen, and K. Mølmer, *Phys. Rev. A* **87**, 023821 (2013).
- [26] C. A. Balanis, *Antenna Theory: Analysis and Design* (Wiley, New York, 2005).
- [27] H. J. Lezec, A. Degiron, E. Devaux, R. A. Linke, L. Martin-Moreno, F. J. Garcia-Vidal, and T. W. Ebbesen, *Science* **297**, 820 (2002).
- [28] J. A. Schuller, T. Taubner, and M. L. Brongersma, *Nat. Photonics* **3**, 658 (2009).
- [29] R. Esteban, T. V. Teperik, and J. J. Greffet, *Phys. Rev. Lett.* **104**, 026802 (2010).
- [30] J. Claudon, J. Bleuse, N. S. Malik, M. Bazin, P. Jaffrennou, N. Gregersen, C. Sauvan, P. Lalanne, and J.-M. Gerard, *Nat. Photonics* **4**, 174 (2010).
- [31] Z. Ruan and S. Fan, *Phys. Rev. Lett.* **105**, 013901 (2010).
- [32] V. E. Lembessis, A. A. Rashed, O. M. Aldossary, and Z. Ficek, *Phys. Rev. A* **88**, 053814 (2013).
- [33] H. Yagi, *Proc. IRE* **16**, 715 (1928).
- [34] A. G. Curto, G. Volpe, T. H. Taminiau, M. P. Kreuzer, R. Quidant, and N. F. van Hulst, *Science* **329**, 930 (2010).
- [35] T. Coenen, E. J. R. Vesseur, A. Polman, and A. F. Koenderink, *Nano Lett.* **11**, 3779 (2011).
- [36] P. Bharadwaj, B. Deutsch, and L. Novotny, *Adv. Opt. Photonics* **1**, 438 (2009).
- [37] N. Engheta, *Science* **317**, 1698 (2007).
- [38] L. Novotny and N. van Hulst, *Nat. Photonics* **5**, 83 (2011).
- [39] B. Paolo, H. Jer-Shing, and H. Bert, *Rep. Prog. Phys.* **75**, 024402 (2012).
- [40] G. Y. Slepyan, Y. D. Yerchak, S. A. Maksimenko, A. Hoffmann, and F. G. Bass, *Phys. Rev. B* **85**, 245134 (2012).
- [41] S. Mokhlespour, J. E. M. Haverkort, G. Slepyan, S. Maksimenko, and A. Hoffmann, *Phys. Rev. B* **86**, 245322 (2012).
- [42] Y. Slepyan and A. Boag, *Phys. Rev. Lett.* **111**, 023602 (2013).
- [43] M. O. Scully and M. S. Zubairy, *Quantum Optics* (Cambridge University Press, Cambridge, 1997).
- [44] R. Loudon, *The Quantum Theory of Light* (Oxford University Press, London, 2000).
- [45] J. F. Liu, M. Zhou, and Z. F. Yu, *Opt. Lett.* **41**, 4166 (2016).
- [46] J. T. Shen and S. Fan, *Phys. Rev. A* **79**, 023837 (2009).
- [47] H. Zheng, D. J. Gauthier, and H. U. Baranger, *Phys. Rev. A* **82**, 063816 (2010).
- [48] D. Roy, *Phys. Rev. Lett.* **106**, 053601 (2011).
- [49] C. Gonzalez-Ballester, E. Moreno, and F. J. Garcia-Vidal, *Phys. Rev. A* **89**, 042328 (2014).
- [50] R. H. Dicke, *Phys. Rev.* **93**, 99 (1954).
- [51] M. O. Scully, *Phys. Rev. Lett.* **102**, 143601 (2009).
- [52] D. W. Wang, R. B. Liu, S. Y. Zhu, and M. O. Scully, *Phys. Rev. Lett.* **114**, 043602 (2015).
- [53] M. P. Hedges, J. J. Longdell, Y. Li, and M. J. Sellars, *Nature (London)* **465**, 1052 (2010).
- [54] M. Hosseini, B. M. Sparkes, G. Campbell, P. K. Lam, and B. C. Buchler, *Nat. Commun.* **2**, 174 (2011).
- [55] Y. H. Chen, M. J. Lee, I. C. Wang, S. Du, Y. F. Chen, Y. C. Chen, and I. A. Yu, *Phys. Rev. Lett.* **110**, 083601 (2013).
- [56] Y. W. Cho *et al.*, *Optica* **3**, 100 (2016).
- [57] L. Verslegers, Z. Yu, P. B. Catrysse, and S. Fan, *J. Opt. Soc. Am. B* **27**, 1947 (2010).
- [58] J. T. Shen and S. Fan, *Opt. Lett.* **30**, 2001 (2005).
- [59] J. T. Shen and S. Fan, *Phys. Rev. A* **76**, 062709 (2007).
- [60] Z. Ficek and R. Tanaś, *Phys. Rep.* **372**, 369 (2002).
- [61] L. Verslegers, Z. Yu, Z. Ruan, P. B. Catrysse, and S. Fan, *Phys. Rev. Lett.* **108**, 083902 (2012).
- [62] A. Svidzinsky, J. T. Chang, and M. O. Scully, *Phys. Rev. A* **81**, 053821 (2010).
- [63] C. T. Claude, D. R. Jacques, and G. Gryberg, *Atom-Photon Interactions: Basic Processes and Applications* (Wiley, New York, 1989).